Research Paper
Computational Methods for Differential Equations
http://cmde.tabrizu.ac.ir
Vol. *, No. *, *, pp. 1-24
DOI:10.22034/cmde.2025.66505.3108

Bifurcation analysis of time-delayed jerk model

Elahe Rafiean Borujeni[1], Javad Alidousti[1,*], and Khayyam Salehi[2]

[1]Department of Applied Mathematics, Faculty of Mathematical Sciences, Shahrekord University, Shahrekord, Iran.

[2]Department of Computer Science, Faculty of Mathematical Sciences, Shahrekord University, Shahrekord, Iran.

Abstract

This paper presents a comprehensive investigation into the dynamic behavior of a time-delayed jerk model. The study introduces an innovative approach to delayed feedback control, thoroughly examining the effects of delay on the system's dynamics. The findings reveal that the presence of delay can lead to the emergence of previously unrecognized dynamic phenomena, such as Hopf, Bautin, and double-Hopf bifurcations. By employing the normal form method, the coefficients for the normal forms of each bifurcation are determined, highlighting that the inclusion of delay significantly increases the system's complexity. Numerical simulations are conducted to validate the effectiveness of the proposed delayed feedback control system, demonstrating its high accuracy in managing complex and nonlinear dynamics. This study offers an in-depth analysis of the system's dynamic behavior while considering two distinct parameters, including co-dimension 1, co-dimension 2 analyses, and the basin of attraction. Poincaré sections and Lyapunov exponents serve as essential tools for exploring the system's dynamic behavior. The findings of this research can assist designers and engineers in effectively addressing delay effects in the design of mechanical and electrical systems, thereby enhancing the performance of dynamic systems.

Keywords. Bifurcation, Hopf, Double-Hopf, Bautin, Delay, Normal form, Lyapunov exponent, Poincaré section.

2010 Mathematics Subject Classification. 37C75, 37G05, 37G15, 37M20.

1. Introduction

In particle motion, the velocity vector and jerk vector are critically important concepts. The third derivative of displacement concerning time, known as "jerk" (or the derivative of acceleration with respect to time) in physics, has been somewhat overlooked. However, jerk plays a vital role in predicting high acceleration over short time intervals, making it essential for the design of mechanisms involved in periodic motions. Additionally, the concept of jerk is relevant in the design of transfer paths that transition gradually from straight sections to circular arcs in railway tracks. Jerk is also significant in road engineering, particularly for determining appropriate curvatures and gradients. By utilizing the third derivative of displacement with respect to time, optimal road gradients for vehicle movement can be established, as well as ideal locations for traffic signs. The application of jerk ultimately contributes to enhanced road safety.

In electronics, the third derivative of current with respect to time, referred to as "current jerk," is instrumental in designing electrical circuits by assessing the acceleration and variations in the speed of electric current. This information enables electronic engineers to optimize circuit designs and mitigate potential interference and issues that may arise during electrical data transmission. For example, in computer systems, incorporating current jerk into the design of cache memories can lead to reduced latency in data access and improved overall system performance. This approach significantly enhances the efficiency of processing units within computer systems. Therefore, analyzing and applying current jerk in electrical circuit design is crucial for improving the efficiency and performance of electronic and computer systems.

Received: 21 March 2025 ; Accepted: 06 October 2025.
∗ Corresponding author. Email: alidousti@sku.ac.ir.

In mechanics, $\dot{x}$ denotes velocity, $\ddot{x}$ signifies acceleration, and $\dddot{x}$ represents jerk. The dynamics of a jerk system are described by a third-order formula of motion that regulates the temporal evolution of a scalar variable x as $\dddot{x} = j(x, \dot{x}, \ddot{x})$.

In this particular context, the symbol j is designated as the jerk function. An example of a basic jerk system is the Coullet system, which may be represented as $\dddot{x} + a\ddot{x} + \dot{x} = g(x)$, in which the function $g(x)$ is nonlinear. Jerk systems can be expressed in the following manner as autonomous three-dimensional systems $\dot{x} = y,\ \dot{y} = z,\ \dot{z} = j(x, y, z)$. Note that distinct dynamics are determined solely by the third equation of the jerk system [23].

This work introduces a proposed jerk differential equation, which is represented as follows:

$$\frac{d^3x}{dt^3} = -ax - b\frac{dx}{dt} - c\frac{d^2x}{dt^2} + (\frac{dx}{dt})^2 + bx\frac{dx}{dt}, \tag{1.1}$$

where the parameters a, b and c are real and a is not equal to zero.

As mentioned, in mechanical systems, the term "jerk" refers to the third derivative of $x(t)$ with regard to t. In the event that the state variables x and y have been established in the following manner: $y = \frac{dx}{dt}, z = \frac{d^2x}{dt^2}$. Therefore the system described by Eq. (1.1) can be regarded as the following jerk system [3]:

$$\begin{cases} \dot{x} = y, \\ \dot{y} = z, \\ \dot{z} = -ax - by - cz + y^2 + bxy, \end{cases} \tag{1.2}$$

With initial conditions $x(0) = x_0, y(0) = y_0, z(0) = z_0$. In many studies, it has been shown that jerk systems can be chaotic (see [1, 7, 9, 12, 13, 24, 26]). It has been widely demonstrated that systems of nonlinear differential equations can experience chaos. In 1963, Lorenz [16] presented a three-dimensional system described by a second-degree polynomial and discovered the initial instance of a chaotic attractor. Subsequently, numerous systems, including Lorenz's, the Lü system [17] and [5, 8, 11], were developed and studied.

A chaotic system is a type of mathematical dynamical system that possesses at least one positive Lyapunov exponent. A chaotic system is characterized by its extreme sensitivity to tiny changes in its initial conditions. For a system's behavior to be chaotic, its variables must include nonlinear terms and possess three characteristics: boundedness, infinite repeatability, and sensitivity to initial conditions [25]. When chaos becomes detrimental, it needs to be controlled. The primary objectives of chaos control are going to be the eradication of chaotic behavior and the stability of the chaotic system at its equilibrium points for the system to be considered stable. On the other hand, due to the occurrence of unexpected events, many of which arising from chaotic systems, controlling chaos is of paramount importance. Control input is added to a chaotic system to eliminate chaos. In situations where chaos is beneficial, chaos can intentionally be induced using the same control methods.

Many control techniques have been discovered and examined. One of the control methods is the delayed feedback control method [2, 4].

Following the implementation of a time-continuous control system, researchers presented the delayed feedback control approach in [30]. By selecting an appropriate time delay, when the desired state to be stabilized is reached, the difference between the current state of the system and its delayed value will converge to zero. Therefore, the method is non-invasive.Moreover, delayed feedback control does not necessitate a reference system, as the control force is derived from the system's intrinsic information. The application of the delayed feedback control method is more effective in regulating chaos inside a continuous dynamic system, as indicated by the principles discussed in reference [32] and other pertinent literature.

Making use of this concept, we incorporate a time-delayed force $k(z(t-\tau) - z(t))$ into system (1.2), resulting in the subsequent control system:

$$\begin{cases} \dot{x} = y, \\ \dot{y} = z, \\ \dot{z} = -ax - by - cz + y^2 + bxy + k(z(t-\tau) - z(t)). \end{cases} \tag{1.3}$$

With $x(0) = x_0, y(0) = y_0, z(0) = z_0$. Stability and evaluation of Hopf, Bautin and double-Hopf bifurcations in a jerk system (1.3) utilizing the delayed feedback control method are the subjects of this paper. For more information about jerk systems, see [6, 10, 14, 15, 20–22, 27–29, 31].

This paper is structured as follows. Section 2 presents the stability analysis of the delayed jerk model. An examination of stability and Hopf bifurcation is conducted for only one equilibrium point. In section 3, Bautin bifurcation analysis for delay-free jerk model is provided. Bautin bifurcation scenarios together with computing the second Lyapunov coefficient for delayed model are achieved in section 4. In furtherance of our analytical findings in section 5, we have demonstrated the existence of double-Hopf bifurcation analysis in time delayed model. Moreover, the coefficients of normal form for these bifurcations are calculated. Section 6 presents the system's behavior, encompassing co-dimension 2, co-dimension 1, and the basin of attraction. This section examines chaotic behavior, periodic and quasi-periodic behaviors, and divergence. A summary is presented in section 7.

2. Stability Analysis of Free-delay Model (1.2)

Presently, we conduct an analysis of the entire system (1.2) that has one equilibrium point $O = (0, 0, 0)$. At point O, the Jacobian matrix of (1.2) is

$$A = \begin{bmatrix} 0 & 1 & 0 \\ 0 & 0 & 1 \\ -a & -b & -c \end{bmatrix},$$

The characteristic equation, however, is

$$P(\lambda) = \lambda^3 + c\lambda^2 + b\lambda + a,$$

when $a > 0, c > 0$ and $bc - a > 0$, equation possesses three negative real part roots, as determined by the Routh–Hurwitz criterion. System (1.2) possesses a stable node or stable spiral. Additionally, the saddle-spiral of (1.2) can be observed using the Routh–Hurwitz criterion, given that $a > 0, c > 0$, and $bc - a < 0$. As per the Routh–Hurwitz criterion, the equilibrium stability region can be identified. Figure 1 illustrates the stability region of the equilibrium in (b, a) plane for $c = 2.5$. The presence of a stable equilibrium is denoted by the gray area in this region. The black curve contains one pair of entirely imaginary eigenvalues denoted by $\pm i\omega, \omega > 0$. The generic Hopf bifurcation points are represented by minus sign symbol and plus sign symbol when both the genericity and transversality conditions for the eigenvalues are met.

2.1. Normal form of the Hopf bifurcation.

To facilitate further analysis, system (1.2) is subsequently reformulated more concisely as:

$$\dot{X} = F(X, \mu), \tag{2.1}$$

where $X = [x, y, z]^T$, $\mu = (b, a)$ represents the bifurcation parameters utilized in the stability and bifurcation analyses, while $F(X, \mu)$ represents the right-hand elements of Eq. (1.2). Throughout the paper for examining Hopf and double-Hopf and Bautin bifurcation, the value $c = 2.5$ is employed in Eq. (1.2). Moreover, the variables for analysis are chosen to be $\mu = \mu(b, a, \tau)$.

In this section, we utilize the method of multiple scales (MMS), a perturbation technique pioneered by Nayfeh [18, 19] for studying nonlinear dynamical systems that exhibit complex temporal or spatial patterns. Unlike conventional methods, MMS introduces distinct variables for different time or spatial scales, allowing for a systematic examination of their interplay and avoiding the emergence of problematic secular terms. By expanding the solution in terms of a small parameter and treating the "fast" and "slow" variations independently, this approach decomposes complicated problems into a sequence of simpler problems that can be solved step by step. As a result, MMS offers a deeper insight into system behavior, accurately representing both rapid oscillations and slow changes in amplitude or frequency—phenomena that are often difficult to capture with traditional techniques.

Instead of treating the solution as a function of just t, we define:

$$T_0 = t, \quad T_1 = \varepsilon \cdot t, \quad T_2 = \varepsilon^2 \cdot t, \cdots, T_k = \varepsilon^k \cdot t.$$

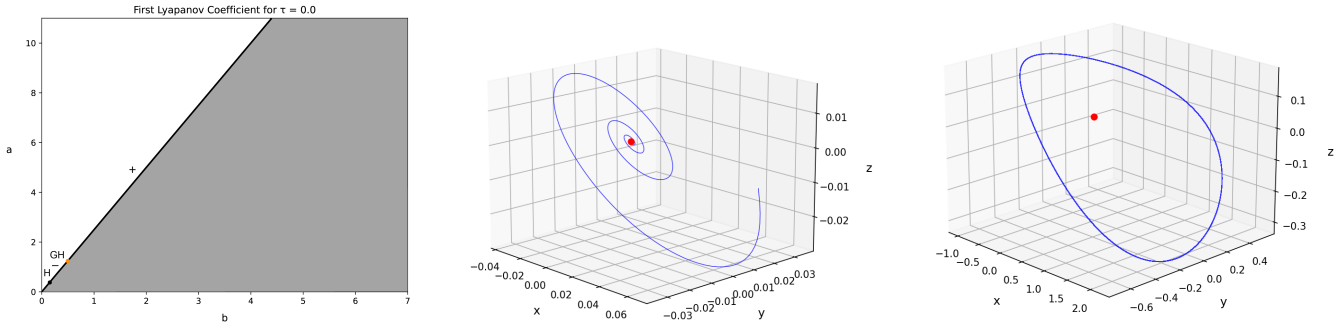

(a) (b) (c)

FIGURE 1. a) The region of stability at origin for the delay-free system ($\tau = 0$). The gray region represents an asymptotically stable parameter domain of equilibrium. At $(b, a, \omega) = (0.1543086, 0.3747494, 0.38716895)$, the selected simple point H (the black point) represents a generic Hopf bifurcation. A Bautin point is denoted by GH (the orange point) that is situated on the boundary point with $(b, a, \omega) = (0.5005005, 1.2512512, 0.7074605)$. At the Bautin point, the bifurcation curve has negative and positive Lyapunov coefficients, determined by minus sign symbol and plus sign symbol. b) The phase space corresponding to parameters in gray area of (a) near point H, showing that equilibrium point is asymptotically stable. c) The phase space corresponding to parameters in white area of (a) near H, as the equilibrium point becomes unstable, a limit stable cycle emerges.

The time derivative becomes:

$$\frac{d}{dt} = \frac{\partial}{\partial T_0} + \varepsilon \cdot \frac{\partial}{\partial T_1} + \varepsilon^2 \cdot \frac{\partial}{\partial T_2} + \cdots .$$

The solution is expanded as a series in powers of ε:

$$X(t;\varepsilon) = X_0(T_0, T_1, T_2, \ldots) + \varepsilon \cdot X_1(T_0, T_1, T_2, \ldots) + \varepsilon^2 \cdot X_2(T_0, T_1, T_2, \ldots) + \mathcal{O}(\varepsilon^3).$$

By substituting this expansion into the differential equation and collecting terms by order of *varepsilon*, we solve sequential equations for $X_0, X_1, X_2, \cdots$, ensuring the elimination of secular terms and capturing both rapid and slow system behaviors. As per the MMS, the solution to Eq. (2.1) can be formally denoted by

$$X(t;\varepsilon) = \sum_{m=1}^{+\infty} \varepsilon^m X_m(T_0, T_1, T_2, \ldots). \tag{2.2}$$

The perturbation analysis uses $\varepsilon \ll 1$ and $T_k = \varepsilon^k t$. For the Hopf bifurcation, Eq. (2.2) is reducible to give:

$$X(t;\varepsilon) = \sum_{m=1}^{3} \varepsilon^m X_m(T_0, T_2). \tag{2.3}$$

No attention is given to the slow scale T_1 as secular terms happen at the third-order layer. For the Hopf bifurcation analysis, we put the parameter b with respect to the primary bifurcation parameter, and its perturbation around b_c is expressed as,

$$b = b_c + \varepsilon^2 b_\varepsilon. \tag{2.4}$$

The coefficient b_ε is considered to be of $O(1)$. By inserting Equations (2.3) and (2.4) into Eq. (2.1) and comparing the coefficients of similar powers of ε, we obtain

$$O(\varepsilon):\ D_0X_1 - AX_1 = 0,$$
$$O(\varepsilon^2):\ D_0X_2 - AX_2 = \frac{1}{2}B(X_1, X_1),$$
$$O(\varepsilon^3):\ D_0X_3 - AX_3 = B(X_1, X_2) + B_{13}(X_1, \mu_\varepsilon) + \frac{1}{6}C(X_1, X_1, X_1) - D_2X_1,$$

where $D_k = \frac{\partial}{\partial T_k}$, $\mu = \mu(b)$ is a bifurcation parameter, A is the variation matrix of Eq. (2.1) evolved at O, and

$$[B(u,v)]_i := \sum_{j,k=1}^{3} \frac{\partial^2 F_i(\xi,\mu)}{\partial\xi_j\partial\xi_k}\Big|_{\xi=O,\mu=\mu_c} u_jv_k,\ i=1,2,3$$
$$[C(u,v,w)]_i := \sum_{j,k,l=1}^{3} \frac{\partial^3 F_i(\xi,\mu)}{\partial\xi_j\partial\xi_k\xi_l}\Big|_{\xi=O,\mu=\mu_c} u_jv_kw_l,\ i=1,2,3$$
$$[B_{13}(u,v)]_i := \sum_{j,k=1}^{3} \frac{\partial^2 F_i(\xi,\mu)}{\partial\xi_j\partial\mu_k}\Big|_{\xi=O,\mu=\mu_c} u_jv_k,,\ i=1,2,3$$

are multilinear functions. The general solution to equation $O(\varepsilon)$ is:

$$X_1(T_0,T_2) = z(T_2)qe^{i\omega T_0} + cc. \tag{2.5}$$

The symbol cc represents the complex conjugate of the phrases that come before it. z represents the amplitude function corresponding to $i\omega$. Let $q \in \mathbb{C}^3$ be the complex eigenvector such that,

$$Aq = i\omega q,\ A\overline{q} = -i\omega\overline{q},$$

additionally, the adjoint eigenvector $p \in \mathbb{C}^3$ possesses the following properties:

$$A^Tp = -i\omega p,\ A^T\overline{p} = i\omega\overline{p},$$

and possessing the following characteristics

$$\langle p, q\rangle = 1,$$

where $\langle p, q\rangle$ is the standard scalar product in $\mathbb{C}^3$. This normalization is possible since the eigenvalues $\pm i\omega$ are simple. Equation (2.5) is substituted into the equation $O(\varepsilon^2)$ to produce

$$(D_0 - A)X_2 = \frac{1}{2}B(q,q)z^2e^{2i\omega_1T_0} + \frac{1}{2}B(q,\overline{q})|z|^2 + cc. \tag{2.6}$$

It is possible to formulate the specific solution of Eq. (2.6) as

$$X_2 = k_{11}z^2e^{2i\omega_1T_0} + k_{1\overline{1}}|z|^2 + cc. \tag{2.7}$$

where

$$k_{11} = \frac{1}{2}(2i\omega I - A)^{-1}B(q,q),$$
$$k_{1\overline{1}} = \frac{-1}{2}A^{-1}B(q,\overline{q}).$$

By substituting Eqs. (2.5) and (2.6) into $O(\varepsilon^3)$ equation and removing secular terms, the differential operator D_2z is obtained.

$$\dot{z} = \langle p, g_1\rangle z + \langle p, (g_{11\overline{1}} + \overline{g_{1\overline{11}}})\rangle z|z|^2, \tag{2.8}$$

where

$$\begin{aligned} g_1 =& B_{13}(q,\mu_\epsilon),\\ g_{11\bar{1}} =& B(q,k_{1\bar{1}}) + B(q,\bar{k}_{1\bar{1}}) + \frac{1}{6}C(q,q,\bar{q}) + \frac{1}{6}C(q,\bar{q},q),\\ g_{1\bar{1}\bar{1}} =& B(q,\bar{k}_{11}) + \frac{1}{6}C(q,\bar{q},\bar{q}). \end{aligned}$$

We deduce that

$$\langle p,(g_{11\bar{1}}+\overline{g_{1\bar{1}\bar{1}}})\rangle = \frac{1}{2}\langle p, C(q,q,\bar{q}) + B(\bar{q},(2i\omega I - A)^{-1}B(q,q)) - 2B(q,A^{-1}B(q,\bar{q}))\rangle.$$

Equation (2.8) can be modified to represent the amplitude of the generic Hopf bifurcation by incorporating $z = \rho e^{i\theta}$, we get

$$\dot{\rho} = \Re\big(\langle p, g_1\rangle\big)\rho + \Re\big(\langle p,(g_{11\bar{1}}+\overline{g_{1\bar{1}\bar{1}}})\rangle\big)\rho^3. \tag{2.9}$$

Furthermore, the phase equation is left out. It is possible to calculate the bifurcating response using Eq. (2.8), and the stability of it is decided by the sign of variable $l_1 = \Re\big(\langle p,(g_{11\bar{1}}+\overline{g_{1\bar{1}\bar{1}}})\rangle\big)$. As an example of a Hopf bifurcating, consider the point H in Figure 1 with $(b_c, a, \omega) = (0.1543086, 0.3747494, 0.3871689)$. It can compute the third-order coefficient in Eq. (2.8). At point H we get $l_1 = -0.0040035$ and $\Re\big(\langle p, g_1\rangle\big) = -0.1955725\ b_\varepsilon$. The theoretical analysis shows that the radius of Hopf bifurcation is $\rho_x \approx 2\sqrt{-48.8493815\ b + 7.5378805}$. It demonstrates the existence of periodic orbits and supercritical Hopf bifurcation. Therefore, cycle is present when $b < b_c$ (see Figure 1(b) and (c)).

In summary, our analysis of the Hopf bifurcation for the jerk model has identified the critical parameter where the system transitions from stable equilibrium to sustained oscillatory behavior. These findings lay the groundwork for understanding more intricate dynamical phenomena that can arise as system parameters are varied, especially in the presence of nonlinear effects and time delay.

3. Bifurcation of the Bautin type in Free-delay Model (1.2)

Having established the conditions for Hopf bifurcation, we now proceed to investigate the Bautin bifurcation. This represents a higher-order degeneracy where the criticality of the Hopf bifurcation changes, allowing for the emergence of multiple limit cycles and more complex dynamic behavior. This analysis provides deeper insight into the richness of the system's oscillatory dynamics, particularly in regions where the first Lyapunov coefficient vanishes.

The determination of the stability and direction of the Hopf bifurcation, specifically whether it is supercritical or sub-critical, is contingent upon the sign of coefficient l_1 in Eq. (2.9). In Figure 1, a critical point GH is identified with the coordinates $(b, a, \omega) = (0.5005005, 1.2512512, 0.7074605)$. This point is additionally denoted by an orange point. The critical point GH clearly separates the curve into two separate sections by different symbols. The curve with minus sign symbol is associated with the negative value of l_1, leading to the occurrence of a supercritical Hopf bifurcation. A stable cycle emerges from the equilibrium point where b is less than b_c. In contrast, the plus sign curve is associated with the positive value of l_1, which gives rise to a sub-critical Hopf bifurcation and the presence of an unstable periodic orbit for values of b greater than b_c.

At the critical point GH where $l_1 = 0$, higher-order terms are need inclusion of Eq. (2.8) to conduct a more in-depth analysis. This situation is referred to the Bautin bifurcation, where two distinct periodic orbits can exist simultaneously. To explore the progression of Bautin bifurcation, it is necessary to include the fifth-order term. Subsequently, the solution to Eq. (2.1) is once again taken as

$$X(t;\varepsilon) = \sum_{m=1}^{5} \varepsilon^m X_m(T_0, T_2, T_4). \tag{3.1}$$

Furthermore, the parameters (b, a) continue to be regarded as the bifurcation parameters. Within close range of the Bautin bifurcation point GH, the perturbation parameters are mathematically represented as:

$$\mu = \mu_c + \varepsilon^4 \mu_\varepsilon. \tag{3.2}$$

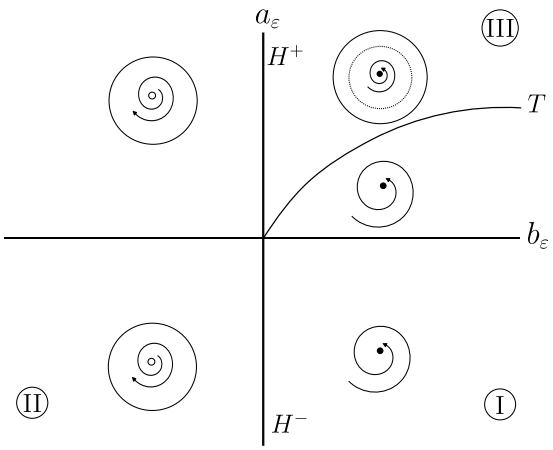

FIGURE 2. Classifying around Bautin point GH.

By inserting Eqs. (3.1) and (3.2) into Eq. (2.1) and comparing the coefficients of similar powers of ε, up to $O(\varepsilon^5)$, by setting $\mu_\varepsilon = \mu_\varepsilon(b_\varepsilon, a_\varepsilon)$, we obtain

$$\dot{\rho} = I_1(b_\varepsilon)\rho + I_{111}(\mu_\varepsilon)\rho^3 + I_5\rho^5. \tag{3.3}$$

The value of the third-order factor I_{111} can be ascertained by analyzing the bifurcation curve in (b, a) plane close by the Bautin bifurcation point. The significance of the fifth-order term factor is approximately computed as $I_5 \approx -0.0039198$ and $I_1(\mu_\varepsilon) \approx -0.1851714\ b_\varepsilon$ around the Bautin point GH. It is evident that the trivial equilibrium of Eq. (3.3) is represented by the solution $\rho = 0$, and the number of nontrivial equilibrium states, namely bifurcating limit cycles, is two. Given that

$$I_1(b_\varepsilon) + I_{111}(\mu_\varepsilon)\rho^2 + I_5\rho^4 = 0,$$

then

$$\rho^2 = \frac{-I_{111}(\mu_\varepsilon) \pm \sqrt{I_{111}^2(\mu_\varepsilon) - 4I_1(b_\varepsilon)I_5}}{2I_5}.$$

Thus, the threshold curves, at which the two separate limit cycles converge at GH, ought to be derived as:

$$I_{111}^2(\mu_\varepsilon) = 4I_1(b_\varepsilon)I_5.$$

Two emerging cycles vanish after colliding in the following curve

$$T = \{(b_\varepsilon, a_\varepsilon) : I_{111}^2(\mu_\varepsilon) - 4I_1(b_\varepsilon)I_5 = 0\}.$$

Figure 2 depicts the state of a stable equilibrium, while it also illustrates the presence of a stable limit cycle and an unstable limit cycle. For better visualization of local bifurcation, the figure is centralized to the origin. If we go from region I to II (from left to right), the stable equilibrium point becomes unstable and a stable limit cycle emerges. In this case, a super-critical Hopf bifurcation occurs. Passing from region II to III, an unstable limit cycle is inserted. Moreover, an unstable equilibrium point turns to stable though sub-critical Hopf bifurcation. In this region, there are two cycles of contrasting stability, which vanish at the curve T via a fold bifurcation that results in a solitary stable equilibrium in region I.

4. Stability Analysis and Bifurcation of the Bautin Type in Delay Model (1.3)

In order to enable more examination, system (1.3) is subsequently reformulated more concisely as:

$$\dot{X} = F(X, X_\tau, \mu), \tag{4.1}$$

where $X = [x, y, z]^T$, μ represents the bifurcation parameters utilized in the stability and bifurcation analyses, while $F(X, X_\tau, \mu)$ represents the right-hand elements of Eq. (1.3). For the succeeding numerical simulations, the following parameters are utilized in Eq. (1.3):

$$k = -1, c = 2.5.$$

Throughout the paper for examining Hopf, double-Hopf, and Bautin bifurcation in delayed case, we set $k = -1, c = 2.5$. Moreover, the variables for analysis are chosen to be $\mu = \mu(b, a, \tau)$. This section examines the impact of time delays dynamic response of (1.3). Discrete delays are selected to emphasize the alterations in the dynamic behavior. The equations for the bifurcation are calculated again using the MMS method.

The variational matrix of system (1.3) assessed at O is $A_0 + A_\tau e^{-\lambda\tau}$, where

$$A_0 = \begin{bmatrix} 0 & 1 & 0 \\ 0 & 0 & 1 \\ -a & -b & -c-k \end{bmatrix},$$

and

$$A_\tau = \begin{bmatrix} 0 & 0 & 0 \\ 0 & 0 & 0 \\ 0 & 0 & k \end{bmatrix}.$$

The corresponding characteristic equation reads

$$D(\lambda, \tau) = \lambda^3 + (c+k)\lambda^2 + b\lambda + a - k\lambda^2 e^{-\lambda\tau} \tag{4.2}$$

If all eigenvalues of Eq. (4.2) have negative real part, then the equilibrium point will be asymptotically stable for $\tau > 0$. By inserting the critical eigenvalue $\lambda = i\omega$, where $\omega > 0$, into Eq. (4.2), and subsequently separating the real and imaginary components, the result is

$$\begin{aligned} R(\omega, b, a, \tau) =& k\,\omega^2 \cos(\omega\tau) - (c+k)\,\omega^2 + a \\ S(\omega, b, a, \tau) =& -k\omega^2 \sin(\omega\tau) - \omega^3 + b\omega \end{aligned} \tag{4.3}$$

and leads to the subsequent polynomial equation:

$$P(\omega) = \omega^6 + \left(c^2 + 2ck - 2b\right)\omega^4 + \left(-2ac - 2ak + b^2\right)\omega^2 + a^2 \tag{4.4}$$

In situations that Eq. (4.4) contains at least one positive real root ω, then Eq. (4.2) possesses a set of entirely imaginary roots $\pm i\omega$, and the point O achieves local asymptotic stability for all values of τ inside the interval $[0, \tau_*)$. When the value of τ exceeds τ_*, the system becomes unstable and there is a possibility of a Hopf bifurcation occurring at $\tau = \tau_*$. The value of τ_* is as follows:

$$\tau_* = \frac{1}{\omega}\begin{cases} \arccos\left(\dfrac{(c+k)\omega^2 - a}{k\,\omega^2}\right) + 2k\pi, & \sin(\omega\tau) \geq 0, \\ 2\pi - \arccos\left(\dfrac{(c+k)\omega^2 - a}{k\,\omega^2}\right) + 2k\pi, & \sin(\omega\tau) < 0, \quad k = 0, 1, \ldots. \end{cases}$$

The determination of the stability boundaries of the equilibrium under varying delays is possible using Eq. (4.3), as illustrated in Figures 3–10. It is worth noting that choosing the value $k = -0.5$ can lead to experience a wider range of stability region. When the value of k is set to -0.5, Figure 11(a) is generated. Moreover, considering parameters τ as a bifurcation parameter yields Figure 11(b). When comparing the outcomes presented in Figure 1 to the stability boundaries of the equilibrium illustrated in Figures 3-10, it becomes evident that the delay exhibits greater complexity. The division of the stability region and the alteration of stability in specific localized regions are characteristics of the novel feature. While the time delay increases, the stability region contracts. The whole Bautin points GHi and double-Hopf points HHi for $\tau = 3, 6$, and 12 are reported in Tables 1 and 2.

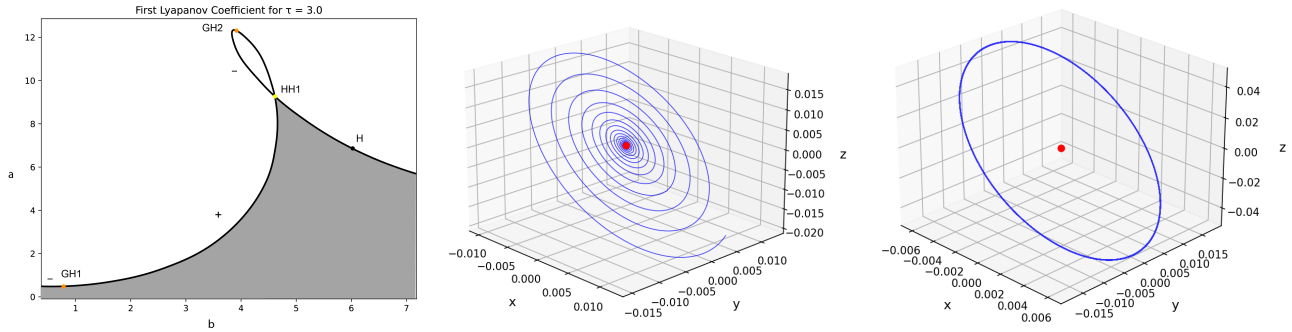

(a) (b) (c)

FIGURE 3. The stability region at the equilibrium point for the system with delay ($\tau = 3$). The gray region represents a parameter domain where equilibrium exhibits asymptotic stability. At $(b, a, \omega) = (5.9198396, 6.9979959, 2.8485025)$, the selected simple point H (the black point) represents a generic Hopf bifurcation. The Bautin points $GH1$ and $GH2$ (the orange points) as well as double-Hopf $HH1$ (the yellow point) are reported in Table 1. The Bautin points separate the bifurcation curve into negative and positive Lyapunov coefficients, determined by minus sign symbol and plus sign symbol. b) The phase space corresponding to parameters in gray area of (a) near point H, showing that equilibrium point is asymptotically stable. c) The phase space corresponding to parameters in white area of (a) near H, as the equilibrium point becomes unstable, a limit stable cycle emerges.

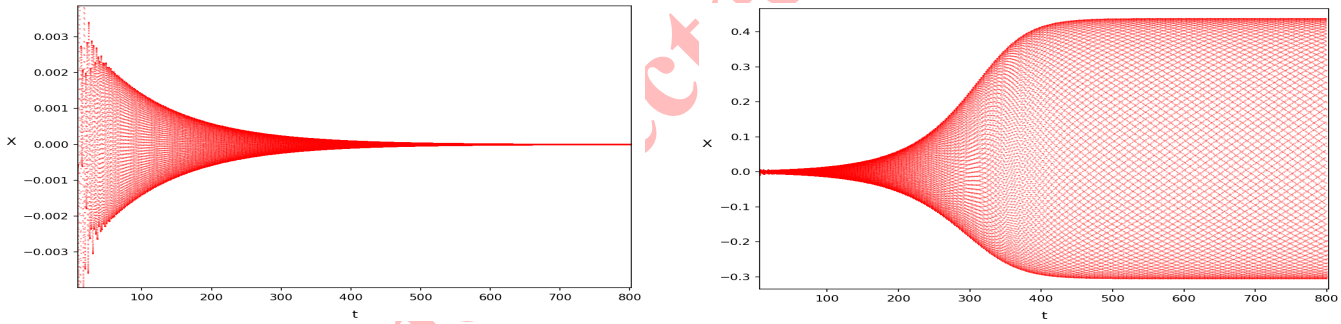

(a) (b)

FIGURE 4. a, b) The time series corresponding to Figure 3(b) and Figure 3(c), respectively.

One of the more recent attributes is the emergence of intersections among the stability boundaries. The parameter values indicate the presence of complex Hopf and double-Hopf phenomena. Delay Hopf bifurcations can be investigated in a manner analogous to the Hopf bifurcation discussed in the preceding section. For the delay case, the coefficient I_{111} in Eq. (3.3) will be computed to identify the presence of the Bautin bifurcation. The number of Bautin and double-Hopf bifurcation points undoubtedly develop as the time delay increases.

4.1. **The second Lyapunov coefficient in delay Bautin normal form.** Bautin bifurcation may occur within the stability boundaries illustrated in Figures 3, 5, and 6, similar to the delay-free scenario. The delay Bautin bifurcations closely mirror the analysis presented in section 3. This section presents the computation of the coefficient $I_{111}(\mu_\varepsilon)$ of the third-order component in Eq. (3.3) to identify Bautin bifurcations, with potential locations indicated by orange points.The number of Bautin bifurcation appears increases with the extension of time delay. For instance, $\tau = 3.0$

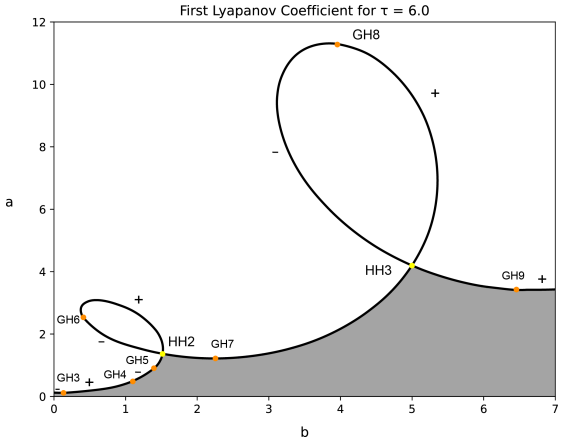

FIGURE 5. The effect of system's delay ($\tau = 6$) in stability region around the interior equilibrium point is depicted. Parameters with asymptotically stable interior equilibrium are in gray. HHi and GHj are double-Hopf and Bautin points in yellow and orange color, respectively, and reported in Table 1.

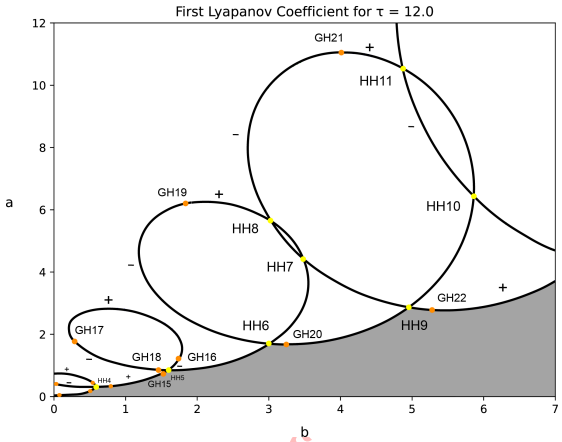

FIGURE 6. The effect of system's delay ($\tau = 12$) in stability region around the interior equilibrium point is demonstrated. Parameters with asymptotically stable interior equilibrium are in gray. HHi and GHj are double-Hopf and Bautin points, and are reported in Table 2.

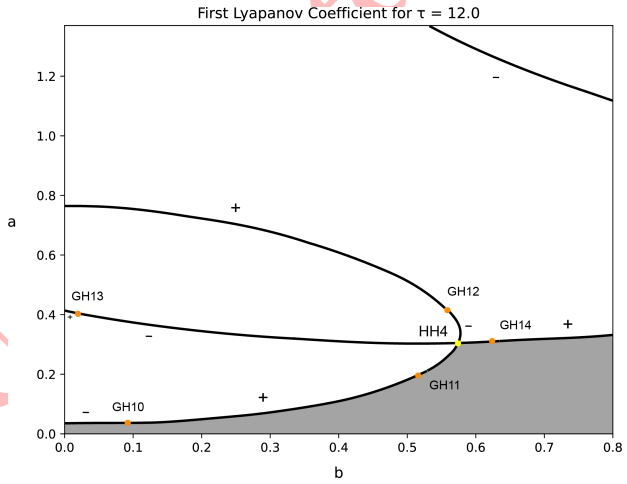

FIGURE 7. The widened region from Figure 6 related to the interior equilibrium point is demonstrated for more clarity. HHi and GHj are double-Hopf and Bautin points, and are reported in Table 2.

is selected to illustrate Bautin bifurcation within the framework of delay. The Bautin point GH_1 , illustrated in the inset of Figure 3(a), is utilized to calculate the coefficient of the fifth-order term. The required fifth-order coefficient I_5 at this point to be approximately $I_5 \simeq -0.0618928$. The negative value of I_5 indicates that the Bautin bifurcation scenario is super-critical. A detailed enumeration of the fifth-order coefficients related to the Bautin point is presented in Table 3, alongside Tables 1 and 2.

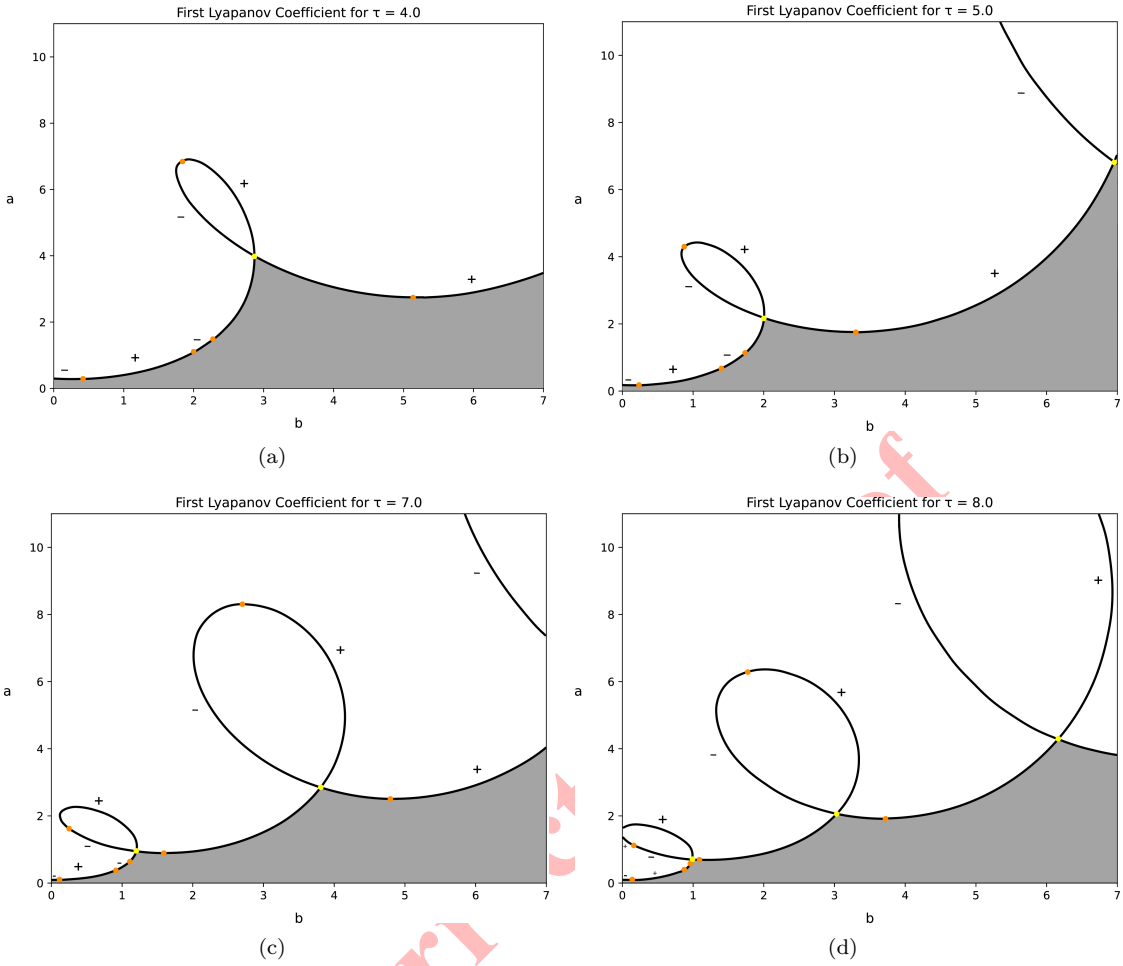

FIGURE 8. Stability region surrounding the interior equilibrium point for $\tau = 4, 5, 7, 8$. Gray indicates asymptotically stable interior equilibrium parameters. The orange and yellow points represent Bautin and double-Hopf bifurcation points, respectively. The Bautin points divide the bifurcation curve into negative and positive Lyapunov coefficients, determined by minus sign symbol and plus sign symbol.

5. Double-Hopf Bifurcation Analysis

Building on the insights gained from the Bautin bifurcation, we now turn our attention to the double-Hopf bifurcation. This phenomenon occurs when two pairs of complex conjugate eigenvalues simultaneously cross the imaginary axis, leading to the possibility of quasi-periodic oscillations and intricate interactions between oscillatory modes. Analyzing the double-Hopf bifurcation enables us to capture and characterize the emergence of even more complex behaviors in the jerk model.

The discovery of crossings among the stability boundaries signifies the emergence of double-Hopf bifurcations, as illustrated in Figures 3-10. These bifurcations are not achievable in the delay-free situation. We have chosen $\tau = 3$, which is represented in Figure 3 denoted by $HH1$ to illustrate double-Hopf bifurcation in the delay case. Another example is associated by $\tau = 6$, which is represented in Figure 5 denoted by $HH3$.

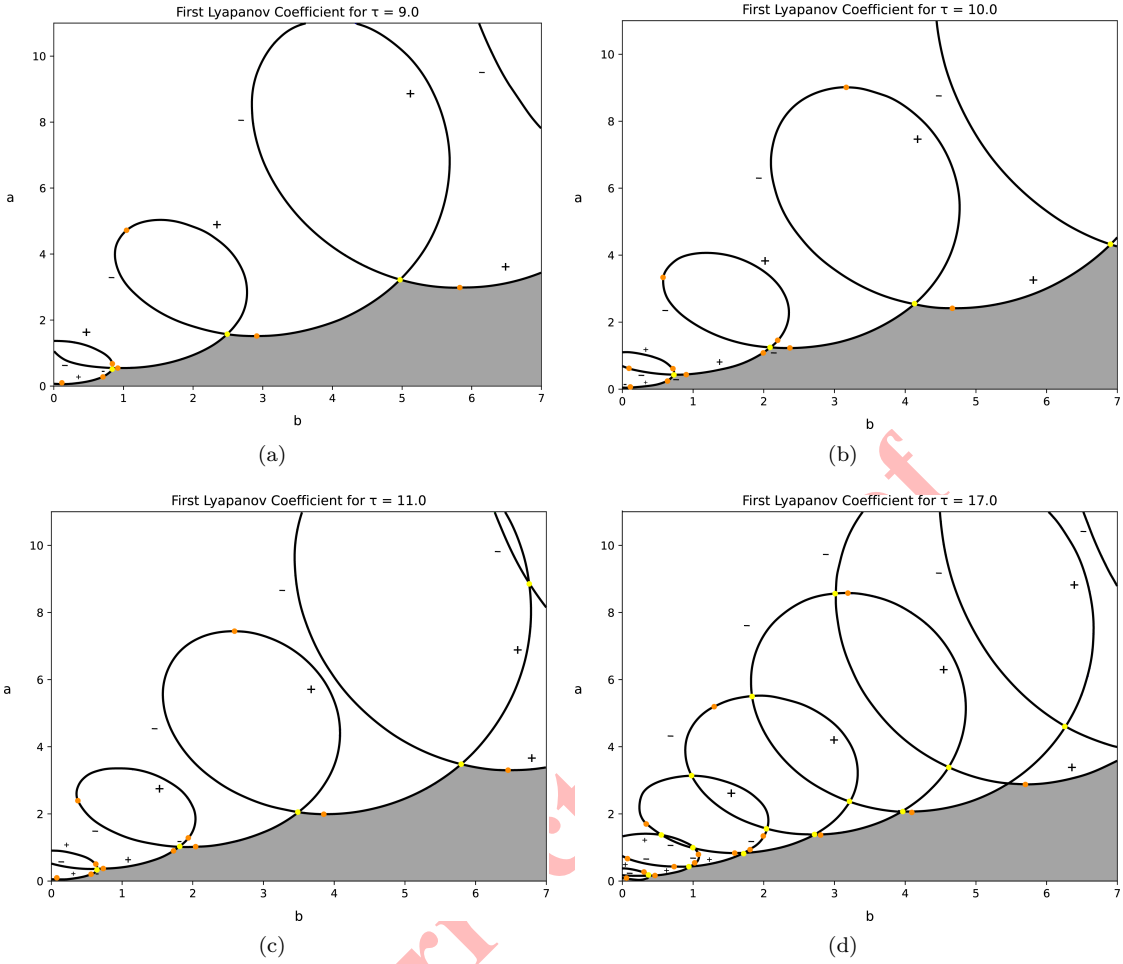

FIGURE 9. The stability region surrounding the interior equilibrium point is shown for $\tau = 9, 10, 11, 17$. The gray indicates asymptotically stable interior equilibrium parameters. The orange and yellow points represent Bautin and double-Hopf bifurcation points, respectively. As the delay increases, the stability regions are more complex.

For the point $HH1$ with $\tau = 3$, the purely imaginary eigenvalues $\pm i\omega_1$ and $\pm i\omega_2$ are computed as:

$$\omega_1 \approx 2.6902935, \ \omega_2 \approx 1.9601691.$$

It represents the double-Hopf bifurcation condition. By choosing another τ (e.g. $\tau = 6$), the purely imaginary eigenvalues $\pm i\omega_1$ and $\pm i\omega_2$ for point $HH3$ are computed as:

$$\omega_1 \approx 2.5225217, \ \omega_2 \approx 1.7985402.$$

If q_j, p_j $(j = 1, 2)$ are the right and left eigenvectors associated with $\pm i\omega_j$, i.e, are the solutions of the following equations:

$$(A_0 + A_\tau e^{-i\omega_j \tau} - i\omega_j I)q_j = 0,$$
$$((A_0 + A_\tau e^{i\omega_j \tau})^T + i\omega_j I)p_j = 0,$$

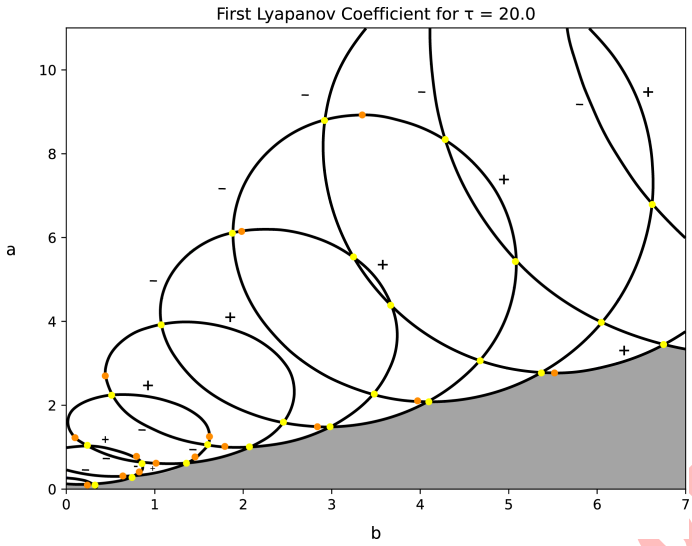

FIGURE 10. The increase of delay complicates the stability region around the interior equilibrium point. This leads to discover more double-Hopf and Bautin points. Furthermore, the stability region contains more interlocking loops.

TABLE 1. The critical points corresponding to the content of Figure 3 and Figure 5.

Point	Type	Coordinate
$GH1$	Bautin	$(b, a, \omega) \approx (0.6584389, 0.4919946, 0.9566369)$
$GH2$	Bautin	$(b, a, \omega) \approx (3.9361702, 12.2596996, 2.3152550)$
$GH3$	Bautin	$(b, a, \omega) \approx (0.2428285, 0.1280853, 0.5160221)$
$GH4$	Bautin	$(b, a, \omega) \approx (1.1300867, 0.5283522, 0.7070055)$
$GH5$	Bautin	$(b, a, \omega) \approx (1.4056037, 0.9366244, 0.7867121)$
$GH6$	Bautin	$(b, a, \omega) \approx (0.4156104, 2.5296864, 1.3152771)$
$GH7$	Bautin	$(b, a, \omega) \approx (2.2788525, 1.2168112, 1.5556488)$
$GH8$	Bautin	$(b, a, \omega) \approx (3.9226150, 11.2955303, 2.1494908)$
$GH9$	Bautin	$(b, a, \omega) \approx (6.5937291, 3.4182788, 2.6055112)$
$HH1$	double-Hopf	$(b, a, \omega_1, \omega_2) \approx (4.6104208, 9.2997995, 2.6902935, 1.9601691)$
$HH2$	double-Hopf	$(b, a, \omega_1, \omega_2) \approx (1.5106276, 1.3713428, 1.3713428, 0.8517666)$
$HH3$	double-Hopf	$(b, a, \omega_1, \omega_2) \approx (4.9958717, 4.1971342, 2.5225217, 1.7985402)$

where $\langle p_j, q_j \rangle = 1,\ j = 1, 2$. Then using the method of the multiple scales method

$$\dot{z_1} = \frac{1}{m_1}\Big((\langle p_1, g_1\rangle - \langle p_1, (i\omega_1\tau_\varepsilon A_\tau e^{-i\omega_1\tau_c})q_1\rangle)z_1$$
$$+ \langle p_1, (g_{11\bar{1}} + \overline{g_{1\bar{1}\bar{1}}})\rangle z_1|z_1|^2 + \langle p_1, (g_{12\bar{2}} + \overline{g_{1\bar{2}\bar{2}}})\rangle z_1|z_2|^2\Big),$$
$$\dot{z_2} = \frac{1}{m_2}\Big((\langle p_2, g_2\rangle - \langle p_2, (i\omega_2\tau_\varepsilon A_\tau e^{-i\omega_2\tau_c})q_2\rangle)z_2$$
$$+ \langle p_2, (g_{22\bar{2}} + \overline{g_{2\bar{2}\bar{2}}})\rangle z_2|z_2|^2 + \langle p_2, (g_{1\bar{1}2} + \overline{g_{1\bar{1}\bar{2}}})\rangle z_2|z_1|^2\Big),$$

TABLE 2. The critical points corresponding to the content of Figure 6 and . 7.

Point	Type	Coordinate
$GH10$	Bautin	$(b, a, \omega) \approx (0.0993987, 0.0364729, 0.2690649)$
$GH11$	Bautin	$(b, a, \omega) \approx (0.5306613, 0.2048096, 0.3836429)$
$GH12$	Bautin	$(b, a, \omega) \approx (0.5707414, 0.4236472, 0.4477269)$
$GH13$	Bautin	$(b, a, \omega) \approx (0.0208416, 0.4096192, 0.7203660)$
$GH14$	Bautin	$(b, a, \omega) \approx (0.6364729, 0.3030060, 0.7871791)$
$GH15$	Bautin	$(b, a, \omega) \approx (1.6671114, 0.8565710, 1.3064622)$
$GH16$	Bautin	$(b, a, \omega) \approx (1.7324883, 1.1767845, 0.9091838)$
$GH17$	Bautin	$(b, a, \omega) \approx (0.2801867, 1.7851901, 1.2000490)$
$GH18$	Bautin	$(b, a, \omega) \approx (1.5223482, 0.7605070, 0.8733113)$
$GH19$	Bautin	$(b, a, \omega) \approx (1.8959306, 6.2201467, 1.6076898)$
$GH20$	Bautin	$(b, a, \omega) \approx (3.2735156, 1.6731154, 1.8292806)$
$GH21$	Bautin	$(b, a, \omega) \approx (4.1420947, 11.0473649, 2.1060386)$
$GH22$	Bautin	$(b, a, \omega) \approx (5.4402935, 2.7698465, 2.3528133)$
$HH4$	double-Hopf	$(b, a, \omega_1, \omega_2) \approx (0.5722861, 0.3042921, 0.7813242, 0.4146577)$
$HH5$	double-Hopf	$(b, a, \omega_1, \omega_2) \approx (1.5867933, 0.8554277, 1.3020431, 0.8820757)$
$HH6$	double-Hopf	$(b, a, \omega_1, \omega_2) \approx (3.0090022, 1.6984246, 1.8188278, 1.3846791)$
$HH7$	double-Hopf	$(b, a, \omega_1, \omega_2) \approx (3.4763690, 4.4471117, 2.2839871, 1.4851096)$
$HH8$	double-Hopf	$(b, a, \omega_1, \omega_2) \approx (3.0335083, 5.6204051, 2.2595078, 1.5321319)$
$HH9$	double-Hopf	$(b, a, \omega_1, \omega_2) \approx (4.9502375, 2.8657164, 2.3376988, 1.8983146)$
$HH10$	double-Hopf	$(b, a, \omega_1, \omega_2) \approx (5.8587146, 6.4396099, 2.8118369, 1.9759818)$
$HH11$	double-Hopf	$(b, a, \omega_1, \omega_2) \approx (4.8679669, 10.5476369, 2.7583929, 2.0707125)$

TABLE 3. The second Lyapunov coefficient associated with the Bautin points

Point	Coordinate	2nd Lyapunov coef.	Type
$GH1$	$(b, a, \omega, \tau) \approx (0.6584389, 0.4919946, 0.9566369, 3)$	-0.0618928	Super-critical
$GH2$	$(b, a, \omega, \tau) \approx (3.9361702, 12.2596996, 2.3152550, 3)$	-12.5456216	Super-critical
$GH3$	$(b, a, \omega, \tau) \approx (0.2428285, 0.1280853, 0.5160221, 6)$	-0.0532859	Super-critical
$GH4$	$(b, a, \omega, \tau) \approx (1.1300867, 0.5283522, 0.7070055, 6)$	1.6047136	Sub-critical
$GH5$	$(b, a, \omega, \tau) \approx (1.4056037, 0.9366244, 0.7867121, 6)$	0.9863922	Sub-critical
$GH6$	$(b, a, \omega, \tau) \approx (0.4156104, 2.5296864, 1.3152771, 6)$	0.0057265	Sub-critical
$GH7$	$(b, a, \omega, \tau) \approx (2.2788525, 1.2168112, 1.5556488, 6)$	-0.8181691	Super-critical
$GH8$	$(b, a, \omega, \tau) \approx (3.9226150, 11.2955303, 2.1494908, 6)$	-0.2522125	Super-critical
$GH9$	$(b, a, \omega, \tau) \approx (6.5937291, 3.4182788, 2.6055112, 6)$	-2.9387006	Super-critical
$GH10$	$(b, a, \omega, \tau) \approx (0.0993987, 0.0364729, 0.2690649, 12)$	-0.0333619	Super-critical
$GH11$	$(b, a, \omega, \tau) \approx (0.5306613, 0.2048096, 0.3836429, 12)$	15.4021195	Sub-critical
$GH12$	$(b, a, \omega, \tau) \approx (0.5707414, 0.4236472, 0.4477269, 12)$	-0.0036876	Super-critical
$GH13$	$(b, a, \omega, \tau) \approx (0.0208416, 0.4096192, 0.7203660, 12)$	-0.0144418	Super-critical
$GH14$	$(b, a, \omega, \tau) \approx (0.6364729, 0.3030060, 0.7871791, 12)$	-0.14129137	Super-critical
$GH15$	$(b, a, \omega, \tau) \approx (1.6671114, 0.8565710, 1.3064622, 12)$	-0.4352336	Super-critical
$GH16$	$(b, a, \omega, \tau) \approx (1.7324883, 1.1767845, 0.9091838, 12)$	1.0345635	Sub-critical
$GH17$	$(b, a, \omega, \tau) \approx (0.2801867, 1.7851901, 1.2000490, 12)$	-0.0005606	Super-critical
$GH18$	$(b, a, \omega, \tau) \approx (1.5223482, 0.7605070, 0.8733113, 12)$	1.1036741	Sub-critical
$GH19$	$(b, a, \omega, \tau) \approx (1.8959306, 6.2201467, 1.6076898, 12)$	-0.0161390	Super-critical
$GH20$	$(b, a, \omega, \tau) \approx (3.2735156, 1.6731154, 1.8292806, 12)$	-1.0078734	Super-critical
$GH21$	$(b, a, \omega, \tau) \approx (4.1420947, 11.0473649, 2.1060386, 12)$	-0.0558478	Super-critical
$GH22$	$(b, a, \omega, \tau) \approx (5.4402935, 2.7698465, 2.3528133, 12)$	-1.8190023	Super-critical

where

$$g_1 = B_{13}(q_1, \mu_\varepsilon) + B_{23}(q_1, \mu_\varepsilon)e^{-i\omega_1\tau_c},$$
$$g_2 = B_{13}(q_2, \mu_\varepsilon) + B_{23}(q_2, \mu_\varepsilon)e^{-i\omega_2\tau_c},$$
$$m_1 = \langle p_1, (\tau_c A_\tau e^{-i\omega_1\tau_c} + I)q_1\rangle,$$
$$m_2 = \langle p_2, (\tau_c A_\tau e^{-i\omega_2\tau_c} + I)q_2\rangle,$$

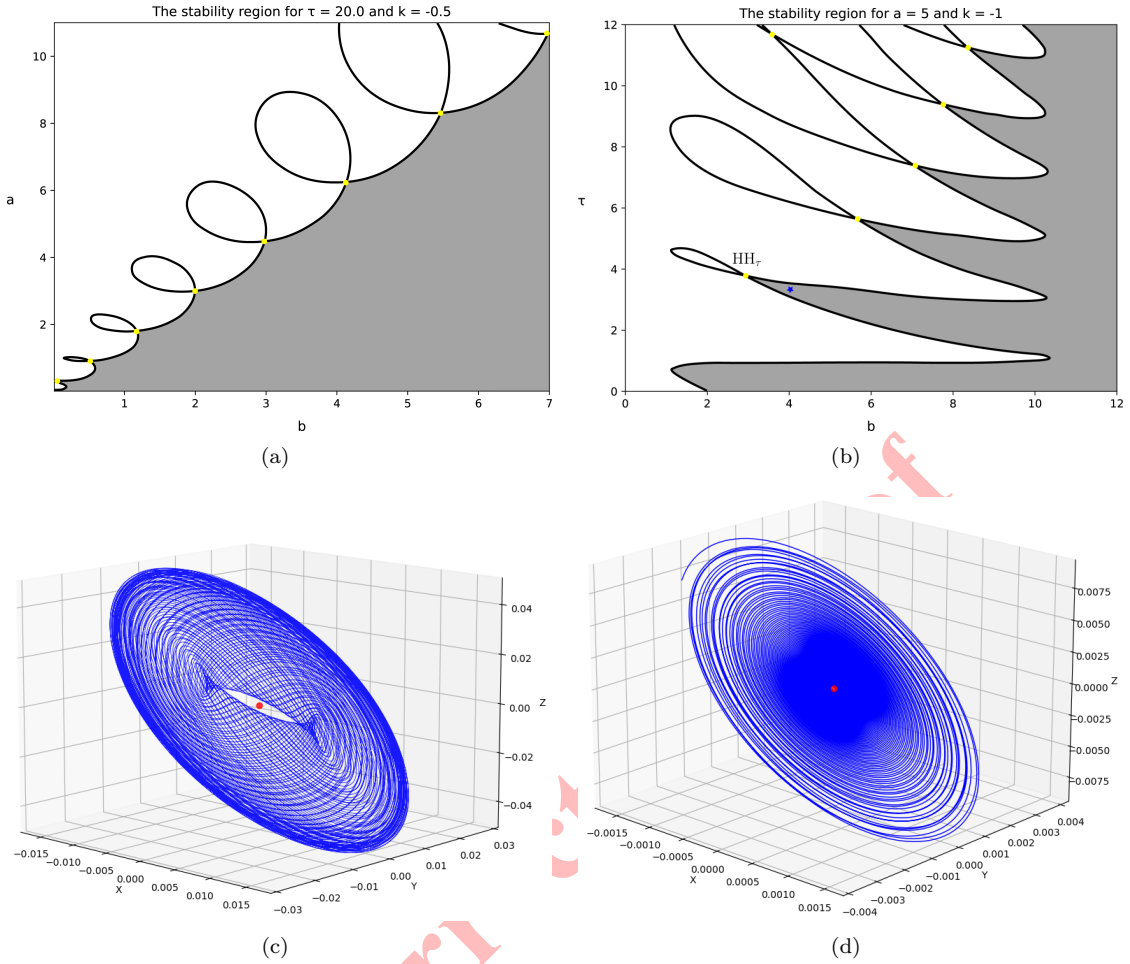

FIGURE 11. a) The stability region corresponding to value $k = -0.5$ can lead to experience a wider range of stability region. b) Considering τ as one of the bifurcation parameters yields another experience of stability region. A critical double-Hopf point HH_τ is determined at $(b, \tau) = (3.2545090, 3.6993988)$. c) The phase space corresponding to parameters near point HH_τ, showing a torus. d) The phase space corresponding to parameters in asymptotic (gray) area of (b) marked by $\star$ at $(b, \tau) = (4, 3.5)$.

in which $\mu = \mu_c + \varepsilon^2 \mu_\varepsilon$, $\mu_\varepsilon = \mu_\varepsilon(b_\varepsilon, a_\varepsilon, \tau_\varepsilon)$, $\mu_c = \mu_c(b_c, a_c, \tau_c)$, and

$$[B_{13}(u,v)]_i := \sum_{j,k=1}^{3} \frac{\partial^2 F_i(\xi, \xi_\tau, \mu)}{\partial \xi_j \partial \mu_k}\Big|_{\xi=O, \xi_\tau=O, \mu=\mu_c} u_j v_k, , \ \ i = 1, 2, 3$$

$$[B_{23}(u,v)]_i := \sum_{j,k=1}^{3} \frac{\partial^2 F_i(\xi, \xi_\tau, \mu)}{\partial (\xi_\tau)_j \partial \mu_k}\Big|_{\xi=O, \xi_\tau=O, \mu=\mu_c} u_j v_k, , \ \ i = 1, 2, 3$$

Furthermore, additional coefficients are determined via Taylor expansion. This equation can be rewrite as:

$$\dot{z_1} = C_1(\mu_\varepsilon)z_1 + C_{11\bar{1}}z_1|z_1|^2 + C_{12\bar{2}}z_1|z_2|^2,$$
$$\dot{z_2} = C_2(\mu_\varepsilon)z_2 + C_{1\bar{1}2}z_2|z_1|^2 + C_{22\bar{2}}z_2|z_2|^2,$$

By substituting $z_i = \rho_i e^{i\theta}, i = 1, 2$, one can express the complex amplitudes as:

$$\begin{aligned} \dot{\rho_1} &= L_1\rho_1 + L_{11\bar{1}}\rho_1^3 + L_{12\bar{2}}\rho_1\rho_2^2, \\ \dot{\rho_2} &= L_2\rho_2 + L_{22\bar{2}}\rho_2^3 + L_{1\bar{1}2}\rho_1^2\rho_2, \end{aligned} \tag{5.1}$$

where $L_i = \Re(C_i(\mu_\varepsilon))$ and $L_{ijk} = \Re(C_{ijk})$. As such, one can derive the equilibrium points of Eq. (5.1):

$$\begin{aligned} &E_0 = (0,0),\ E_1 = (\sqrt{\frac{-L_1}{L_{11\bar{1}}}}, 0),\ E_2 = (0, \sqrt{\frac{-L_2}{L_{22\bar{2}}}}), \\ &E_3 = \Big(\sqrt{\frac{L_2L_{12\bar{2}} - L_1L_{22\bar{2}}}{L_{11\bar{1}}L_{22\bar{2}} - L_{1\bar{1}2}L_{12\bar{2}}}}, \sqrt{\frac{L_1L_{1\bar{1}2} - L_2L_{11\bar{1}}}{L_{11\bar{1}}L_{22\bar{2}} - L_{1\bar{1}2}L_{12\bar{2}}}}\Big). \end{aligned} \tag{5.2}$$

E_0 represents the equilibrium of Eq. (5.1) with no action, whereas E_1 and E_2 represent periodic behaviors with frequencies of ω_1 and ω_2, accordingly. E_3 denotes a quasi-periodic motion of Eq. (5.1). The Jacobian matrix of Eq. (5.1) is provided as follows:

$$A_\rho = \begin{bmatrix} L_1 + 3L_{11\bar{1}}\rho_1^2 + L_{12\bar{2}}\rho_2^2 - \lambda & 2L_{12\bar{2}}\rho_1\rho_2 \\ 2L_{1\bar{1}2}\rho_1\rho_2 & L_2 + L_{1\bar{1}2}\rho_1^2 + 3L_{22\bar{2}}\rho_2^2 - \lambda \end{bmatrix}_{(\rho_1,\rho_2)}.$$

Analyzing the eigenvalues of A_ρ at the equilibrium allows one to ascertain the stability of the equilibrium points.

Example 5.1. To analyze the double-Hopf bifurcations in system (1.3), the constant delay of $\tau = 3$ is utilized as an illustration. The parameter $\mu_0(b_0, a_0, \tau_0)$ is assumed to be constant at $(b_0, a_0, \tau_0) \approx (4.6104208, 9.2997995, 3)$; this value corresponds to the intersection point $HH1$ in Figure 3 as well. It is possible to derive the coefficients of Eq. (5.1) that correspond to the bifurcation point $HH1$, and the equilibrium points specified in Eq. (5.2) are as follows:

$$\begin{aligned} &L_1 \approx -0.4517428\,\tau_\varepsilon - 0.0107214\,a_\varepsilon - 0.1367348\,b_\varepsilon, \\ &L_{11\bar{1}} \approx 0.3103871, \\ &L_{12\bar{2}} \approx 1.0896151, \\ &L_2 \approx 0.5328539\,\tau_\varepsilon + 0.0346225\,a_\varepsilon + 0.0805686\,b_\varepsilon, \\ &L_{1\bar{1}2} \approx -0.3938235, \\ &L_{22\bar{2}} \approx -0.4391840, \\ &E_0 = (0,0), \\ &E_1 = (\sqrt{1.4554174\,\tau_\varepsilon + 0.0345422\,a_\varepsilon + 0.4405300\,b_\varepsilon}, 0), \\ &E_2 = (0, \sqrt{1.2132817\,\tau_\varepsilon + 0.0788338\,a_\varepsilon + 0.1834507\,b_\varepsilon})), \\ &E_3 = (\sqrt{1.3053578\,\tau_\varepsilon + 0.1127618\,a_\varepsilon + 0.0947307\,b_\varepsilon}, \sqrt{0.0427459\,\tau_\varepsilon - 0.0222815\,a_\varepsilon + 0.0985041\,b_\varepsilon}). \end{aligned}$$

The numerical simulation corresponding near the point $HH1$ is depicted in Figure 12(a).

Example 5.2. To analyze another double-Hopf bifurcation in system (1.3), the constant delay of $\tau = 6$ is utilized as an illustration. The parameter $\mu_0(b_0, a_0, \tau_0)$ is assumed to be constant at $(b_0, a_0, \tau_0) = (4.9958717, 4.1971342, 6)$; this value corresponds to the intersection point $HH3$ in Figure 5 as well. It is possible to derive the coefficients of Eq. (5.1)

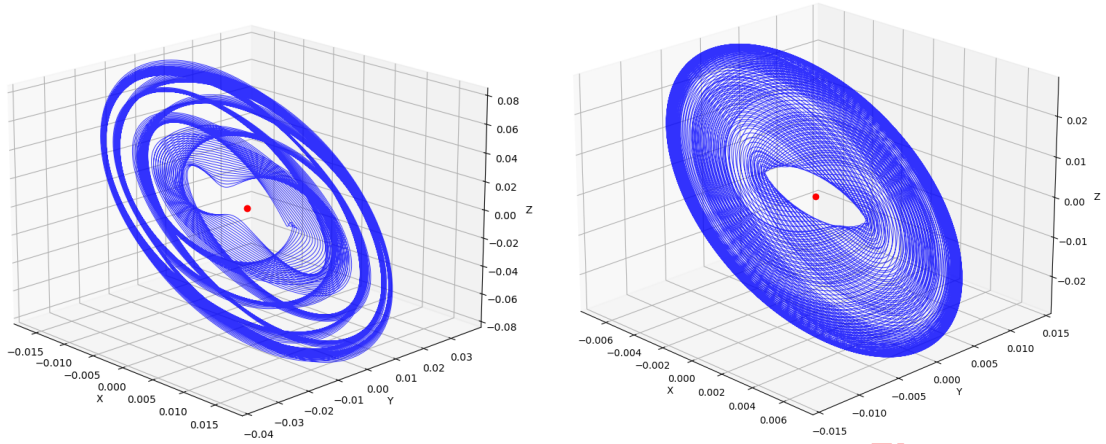

(a) (b)

FIGURE 12. a) The phase space near the point $HH1$, b) The phase space near the point $HH3$.

that correspond to the bifurcation point $HH3$, and the equilibrium points specified in Eq. (5.2) are as follows:

$$L_1 \approx -0.0584179\,\tau_\varepsilon + 0.0171727\,a_\varepsilon - 0.0600969\,b_\varepsilon,$$
$$L_{11\bar{1}} \approx 0.3242904,$$
$$L_{12\bar{2}} \approx 1.2688926,$$
$$L_2 \approx 0.0656549\,\tau_\varepsilon + 0.0198472\,a_\varepsilon + 0.0200129\,b_\varepsilon,$$
$$L_{1\bar{1}2} \approx -0.3791212,$$
$$L_{22\bar{2}} \approx -0.2626690,$$
$$E_0 = (0, 0),$$
$$E_1 = (\sqrt{0.1801409\,\tau_\varepsilon - 0.0529547\,a_\varepsilon + 0.1853182\,b_\varepsilon}, 0),$$
$$E_2 = (0, \sqrt{0.2499532\ ,\tau_\varepsilon + 0.0755599\,a_\varepsilon + 0.0761908\,b_\varepsilon}),$$
$$E_3 = (\sqrt{0.1716783\,\tau_\varepsilon + 0.0750089\,a_\varepsilon + 0.0242716\,b_\varepsilon}, \sqrt{0.0021627\,\tau_\varepsilon - 0.0327036\,a_\varepsilon + 0.0411586\,b_\varepsilon}).$$

The confirmation of the phase space for this scenario is depicted in Figure 12(b).

6. Analysis of the Model's Performance with Two Distinct Variables

Comprehending the dynamic behavior within the state-parameter space is essential for the most effective layout and motion regulation of systems. This section presents a detailed analysis of the system's two-parameter dynamics, focusing on two primary indices: Lyapunov exponents and Poincaré sections. The analysis of various system responses within the two-parameter plane indicates that the intricacy of the evolutionary process might markedly increase with increased delay. The path-following method and time-domain integration technique are utilized to analyze the intricacies inherent in processes of evolution. The modifications of the basin of attraction are analyzed in the initial conditions plane to illustrate the observed multi-stability phenomena and turbulent transitions.

Monitoring global system dynamics within parameter and state spaces defined by inherent time delay is essential for improving understanding of the system. This section is based on numerical simulation, concentrating on the computation and identification of global dynamic behaviors in the comprehensive evolution of nonlinear dynamic systems with delay, and demonstrates complex dynamic interrelations. In dynamical systems characterized by temporal delays and significant nonlinearity, accurate analytical solutions are largely unattainable, making direct numerical

integration a crucial method for addressing complex functional differential equations. This section employs the fourth-order Runge-Kutta method in conjunction with a fixed step size 0.01 and linear interpolation technique to address the delayed differential equation.

Lyapunov exponent functions serve as a dependable measurement for the quantitative classification of various system responses. In an autonomous dynamical system, a negative largest Lyapunov exponent (LLE) indicates that the system is in a state of equilibrium. When positive LLE occurs, chaotic oscillation arises in the system's response. In the situation that LLE is equal to zero, the system will exhibit periodic or quasi-periodic action. LLE has garnered significant interest owing to its improved effectiveness in identifying various dynamic responses. The calculation of LLE is performed using the subsequent formula:

$$LLE = \lim_{n\longrightarrow\infty}\lim_{\varepsilon\longrightarrow 0}\frac{1}{nh}\sum_{i=1}^{n}\ln\frac{d_i}{\varepsilon},$$

where h represents the integral step size and n signifies the total number of iterations. d_0 specifies the initial distance between two proximate phase trajectories, whereas the notation ε signifies the initial distance between two adjacent phase trajectories. d_i denotes the evolutionary distance between two trajectories at the i-th iteration. In this paper, ε and h are set to 10^{-5} and 0.01, respectively.

LLE will assist the difference between equilibrium points and chaotic actions. Equilibrium points occur when the Lyapunov Exponent (LLE) is less than a small positive constant, while chaos is signified by an LLE above that small positive constant. Periodic responses are deemed simple if the absolute quantity of LLE is below than or equal to small positive constant. Supplementary system responses, including extended periodic and quasi-periodic feedback, are categorized and shown employing different colors for clarity.

Alongside Lyapunov exponents, the Poincaré section is commonly employed to identify diverse system responses. The presence of multiple irregular discrete points in the Poincaré section indicates chaotic oscillations. Upon observing a closed curve in the Poincaré section, the system demonstrates quasi-periodic oscillations. A periodic oscillation is evident in the system response when a finite number of points are examined on the cross-section. This section designates the Poincaré section as the locus of zero angular velocity, defined as follows:

$$P = \Big\{(x_0, y_0, z_0, \ldots, x_{n_\tau}, y_{n_\tau}, z_{n_\tau}) \in \mathbb{R}^{3(n_\tau+1)} : y_0 = 0, \dot{y_0} > 0\Big\},$$

where $n_\tau = \frac{\tau}{h}$. The Poincaré section is typically used for categorizing various periodic behaviors in a two-parameter structure and for illustrating a single-parameter bifurcation diagram.

Our study partitions the (b, a) two-parameter plane to enhance computing efficiency. The LLE and the number of intersection points on the Poincaré section are computed and subsequently used to categorize the system's motion, with results depicted in Figures 13-15. Ten colors represent various types of motion: "D" indicates diverging responses, "C" denotes chaotic motions, "A" signifies asymptotic stability around equilibrium points, "P-1" through "P-6" correspond to period 1 to 6 responses, respectively, as well as "P>" refers to extended periodic and quasi-periodic motions.

The previous sections reveal that the equilibrium point may lose its stability primarily due to Hopf bifurcation. Moreover, the complex structures depicted in the white region of the two-parameter plane related to Figure 1(a) and Figures 3–10 for some τ are also identified and depicted in Figures 13–15. The numerical findings depicted in the figures yield novel insights with different patterns. Multiple kinds of periodic responses, chaotic movements, and divergence are presented. In addition chaotic motion, more periodic responses can be seen in the two-parameter plane, where equilibrium becomes unstable.

To enhance understanding of the two-parameter results obtained, it is essential to conduct a single-parameter bifurcation analysis to locate the bifurcations. Figures 13(b) and (c), as well as Figure 14(b) illustrate the co-dimension 1 for various values of τ when the bifurcation parameter b is selected. For $\tau = 0$ and $a = 1.05$, the co-dimension 1 is illustrated in Figure 13(b). The figure illustrates that the system demonstrates intricate behavior. The red dots represent the relevant outcomes based on the chosen Poincaré section showing only minimum Z values. For a slightly greater value of a ($a = 1.1$), a divergence behavior is identified in Figure 13(c).

The basin of attraction for various initial points is illustrated in Figures 16–17. For parameters $(b, a, \tau) = (0.097, 1.078, 0)$, P-4 type of periodic response and divergence behaviors emerge in spiral pattern. The equilibrium

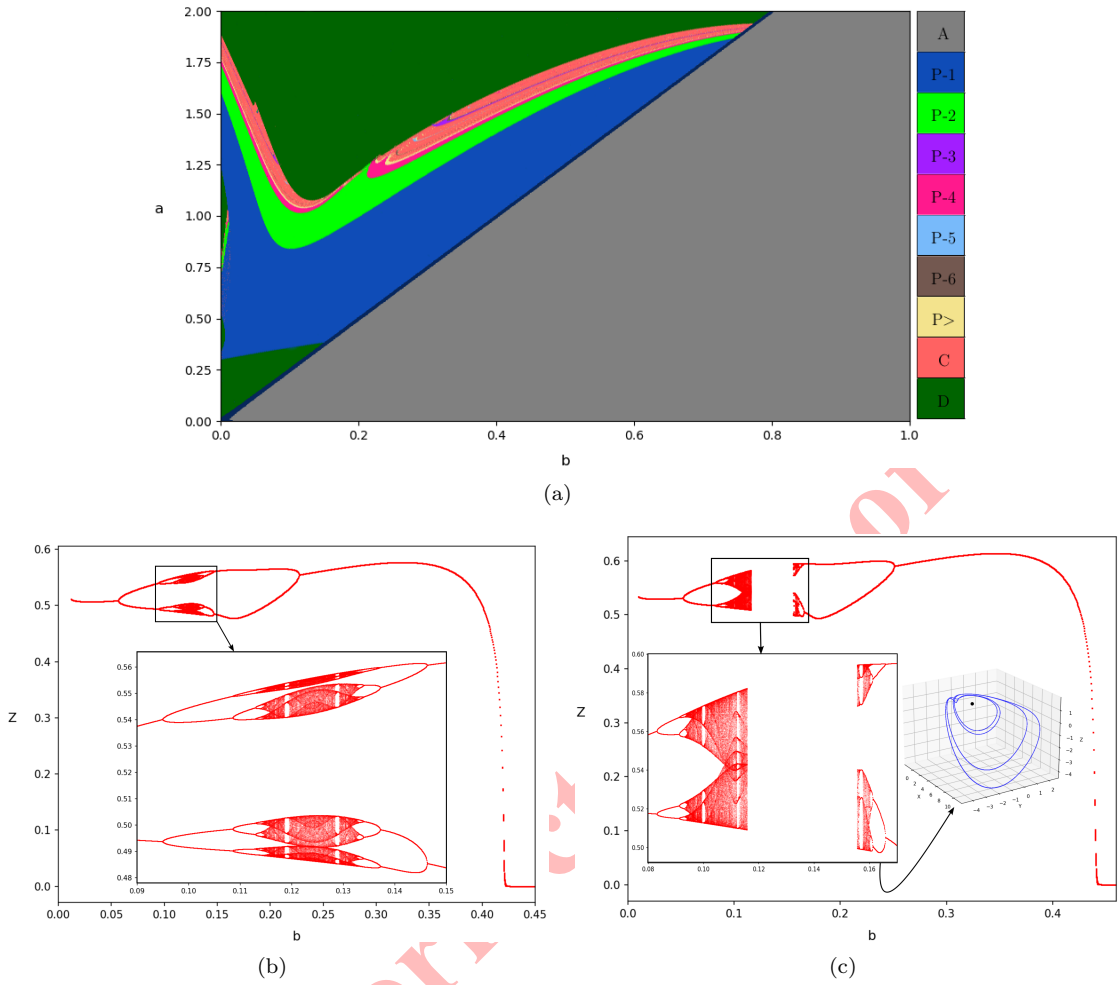

FIGURE 13. a) Co-dimension 2 plane for $\tau = 0$ with parameters (b, a). b) Co-dimension 1 bifurcation diagram in the case of $(a, \tau) = (1.05, 0)$ showing only minimum Z values, c) Co-dimension 1 bifurcation diagram in the case of $(a, \tau) = (1.1, 0)$ showing only minimum Z values together with the phase space at coordinate $(b, a, \tau) = (0.164, 1.1, 0)$ near the equilibrium point demonstrating a period 4 bifurcation.

points are depicted with red dots. As the starting point shifts away from the equilibrium point concerning X and Z, the system begins to diverge. The same pattern is emerged with parameters $(b, a, \tau) = (0.1, 1.078, 0)$, except the higher periodic behavior (P>) is occurred.

Figure 17 illustrates the basin of attraction for different values of parameters and τ, showing periodic, quasi-periodic, chaotic, and divergence behavior of the system.

7. Conclusion

Primarily, this paper intends to demonstrate how delay affects the jerk model, with a particular focus on the role of bifurcations in shaping the system's response. An analysis was carried out to compare the operation of systems with and without delays. The results indicated that the appearance of delay brings novel phenomena, such as a reduction of the region of stability and an escalation in the richness of stability boundary structures. Utilizing the method of multiple scales, the coefficients of the Hopf, Bautin and double-Hopf bifurcation in the normal form are

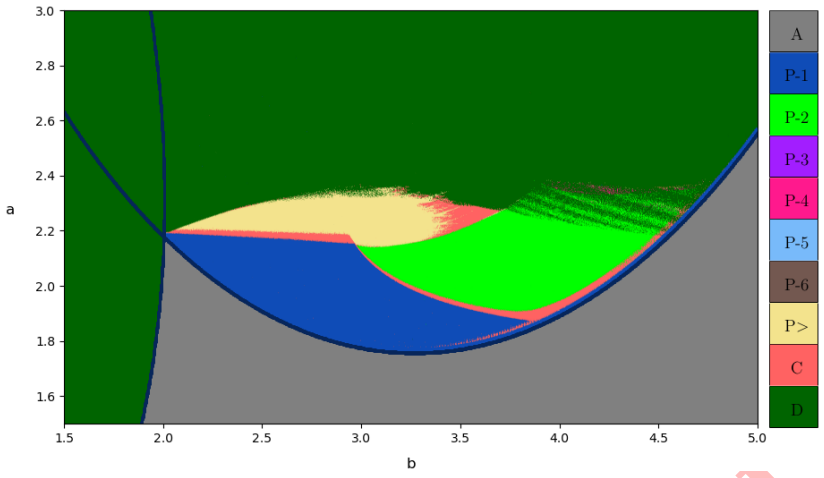

(a)

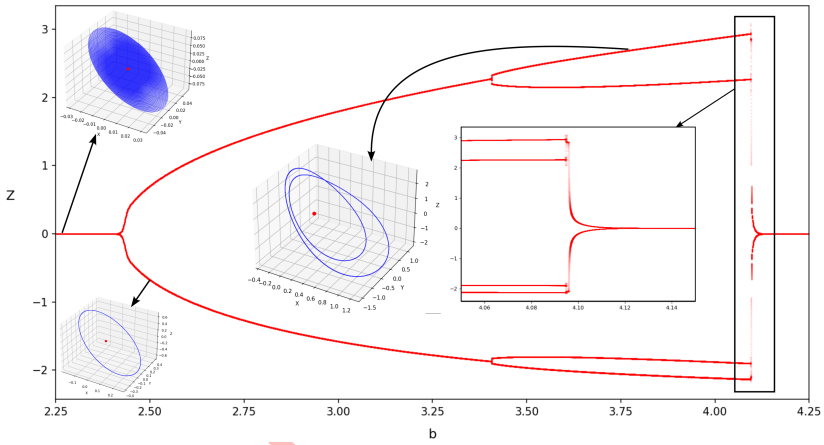

(b)

FIGURE 14. a) Co-dimension 2 plane for $\tau = 5$ with parameters (b, a), b) Co-dimension 1 bifurcation diagram in the case of $(a, \tau) = (1.95, 5)$ together with the phase space near the equilibrium point demonstrating an asymptotically, period 1, and period 2 bifurcation.

computed. Several Bautin and double-Hopf points accumulate within a range of delay levels. As the delay value increases, an increasing number of Bautin and double-Hopf points are identified. Two of the double-Hopf bifurcation points are regarded as taste. These points are validated through the utilization of numerical simulations. A thorough analysis of the system's dynamic behavior regarding two parameters has been conducted, encompassing co-dimension 1, co-dimension 2, and the basin of attraction, employing Lyapunov exponents and Poincaré sections. The bifurcation analysis of the time-delayed jerk system provides valuable physical insights into how dynamic behaviors emerge and evolve in systems. The identification of Hopf bifurcations marks the transition from steady and predictable motion, where velocity, acceleration, and jerk settle to constant values, to sustained oscillatory dynamics, manifesting as rhythmic fluctuations in these physical quantities. The presence of Bautin bifurcations reveals regions in parameter space where multiple oscillatory states can coexist. This indicates that the system may exhibit either small or large amplitude oscillations in velocity, acceleration, and jerk depending on initial conditions. The discovery of double-Hopf bifurcations, enabled by the inclusion of time delay, points to the possibility of even more complex behaviors,

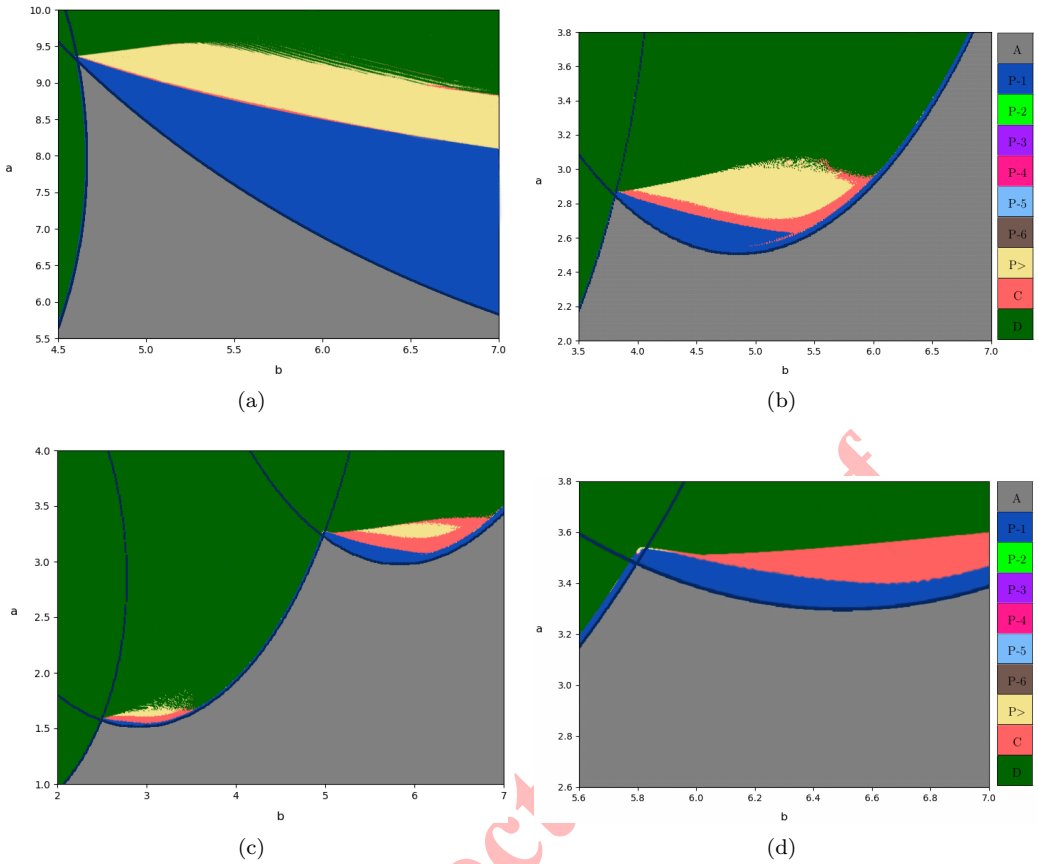

FIGURE 15. Co-dimension 2 plane with parameters (b, a) for a) $\tau = 3$, b) $\tau = 7$, c) $\tau = 9$, d) $\tau = 11$.

such as quasi-periodic or modulated oscillations, where multiple frequencies interact and produce intricate patterns in the system's motion. As the delay increases, the system becomes more susceptible to instability and chaotic responses, making the velocity, acceleration, and jerk increasingly unpredictable. These findings underscore the critical importance of understanding and controlling bifurcation phenomena in practical applications, as they directly impact the stability and safety of systems subject to delayed feedback and nonlinear effects.

ACKNOWLEDGMENT

The authors declare that no funds, grants, or other support were received during the preparation of this manuscript. The authors have no relevant financial or non-financial interests to disclose.

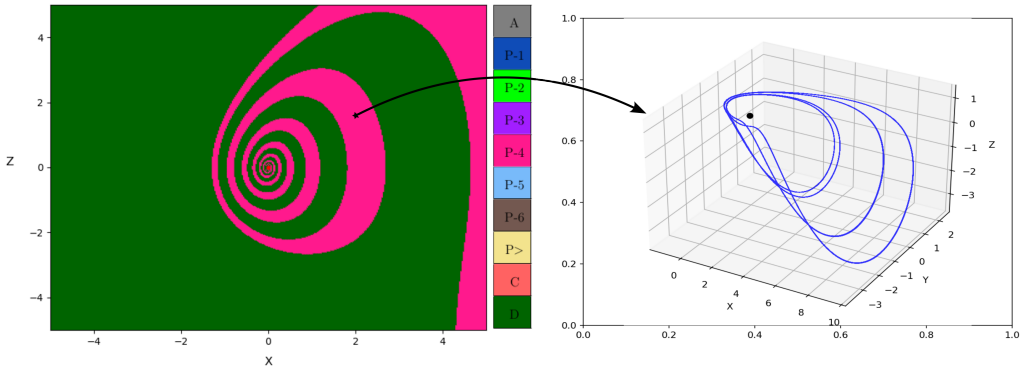

(a)

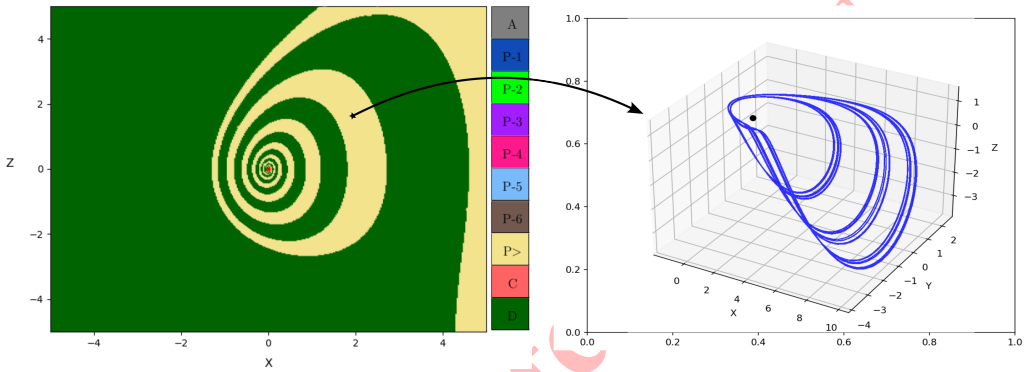

(b)

FIGURE 16. Basin of attraction together with the phase space for a) $(b, a, \tau) = (0.097, 1.078, 0)$, b) $(b, a, \tau) = (0.1, 1.078, 0)$

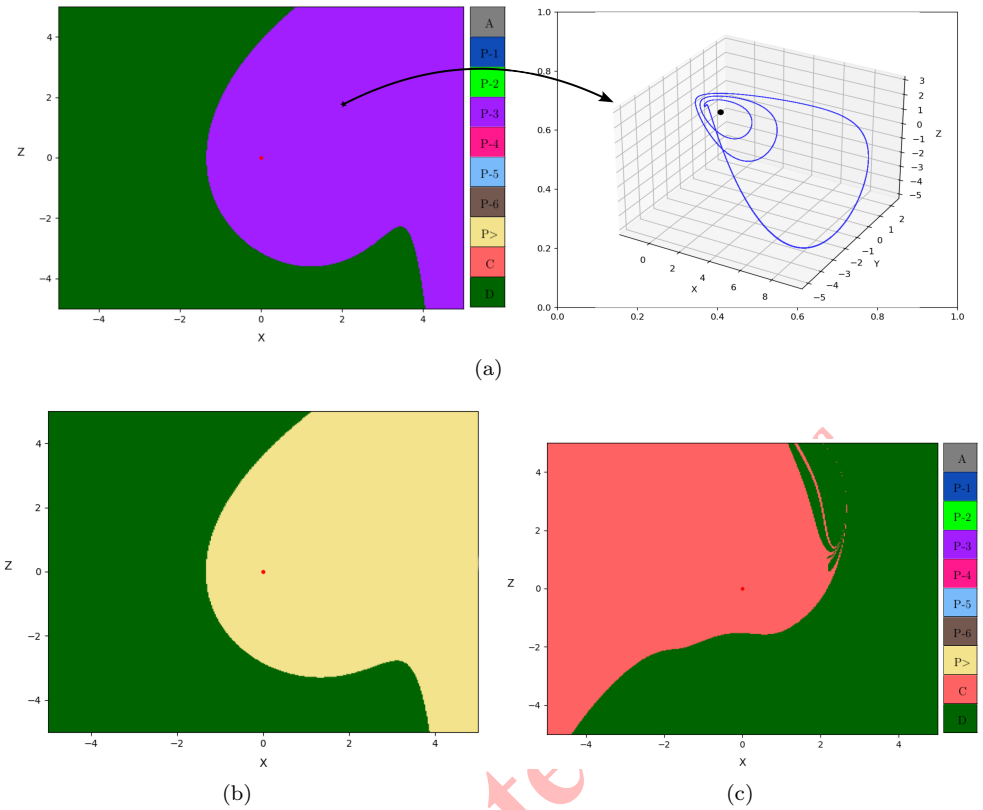

(a)

(b) (c)

FIGURE 17. Basin of attraction for a) $(b, a, \tau) = (1.4711, 0.33, 0)$ with phase space, b) $(b, a, \tau) = (1.261, 0.2462, 0)$, c) $(b, a, \tau) = (3.6, 2.24, 5)$.

REFERENCES

[1] A. B. Alzahrani, M. A. Abdoon, M. Elbadri, M. Berir, and D. E. Elgezouli, *A comparative numerical study of the symmetry chaotic jerk system with a hyperbolic sine function via two different methods*, Symmetry, *15*(11) (2023), 1991.

[2] B. R. Andrievskii and A. L. Fradkov, *Control of chaos: methods and applications. I. methods*, Autom. Remote Control, *64* (2003), 673–713.

[3] T. Bonny, S. Vaidyanathan, A. Sambas, K. Benkouide, W. Al Nassan, and O. Naqaweh, *Multistability and bifurcation analysis of a novel 3D jerk system: Electronic circuit design, FPGA implementation, and image cryptography scheme*, IEEE Access, *11*(2023), 78584–78600.

[4] L. P. Chaintron and A. Diez, *Propagation of chaos: a review of models, methods and applications. II. applications*, arXiv preprint arXiv:2106.14812, (2021).

[5] J. L. Fernandez-Solis, *Building construction: A deterministic non-periodic flow–a case study of chaos theories in tracking production flow*, Architectural engineering and design management, *9*(1) (2013), 21–48.

[6] H. A. Hosham, *Nonlinear behavior of a novel switching jerk system*, Internat. J. Bifur. Chaos, *30*(14) (2020), 2050202.

[7] X. Hu, B. Sang, and N. Wang, *The chaotic mechanisms in some jerk systems*, AIMS Math, *7* (2022), 15714–15740.

[8] C. Hu, Q. Wang, X. Zhang, Z. Tian, and X. Wu, *A new chaotic system with novel multiple shapes of two-channel attractors*, Chaos Solitons Fractals, *162* (2022), 112454.

[9] S. Jafari and J. Sprott, *Simple chaotic flows with a line equilibrium*, Chaos Solitons Fractals, *57* (2013), 79–84.

[10] L. K. Kengne, S. S. Muni, J. C. Chedjou, and K. Kyandoghere, *Various coexisting attractors, asymmetry analysis and multistability control in a 3d memristive jerk system*, The European Physical Journal Plus, *137*(7) (2022), 848.
[11] O. Kozlovska, F. Sadyrbaev, and I. Samuilik, *A new 3d chaotic attractor in gene regulatory network*, Mathematics, *12*(1) (2023), 100.
[12] K. Lamamra, S. Vaidyanathan, W. Putra, E. Darnila, A. Sambas, et al., *A new 3-D chaotic jerk system with four nonlinear terms, its backstepping synchronization and circuit simulation*, in Journal of Physics: Conference Series, *1477*, IOP Publishing, 2020, 022017.
[13] B. Li, B. Sang, M. Liu, X. Hu, X. Zhang, and N. Wang, *Some jerk systems with hidden chaotic dynamics*, Internat. J. Bifur. Chaos, *33*(06) (2023), 2350069.
[14] F. Li and J. Zeng, *Multi-scroll attractor and multi-stable dynamics of a three-dimensional jerk system*, Energies, *16*(5) (2023), 2494.
[15] M. Liu, B. Sang, N. Wang, and I. Ahmad, *Chaotic dynamics by some quadratic jerk systems*, Axioms, *10*(3) (2021), 227.
[16] E. N. Lorenz, *Deterministic nonperiodic flow*, Journal of atmospheric sciences, *20*(2) (1963), 130–141.
[17] J. Lü and G. Chen, *A new chaotic attractor coined*, Internat. J. Bifur. Chaos, *12*(03) (2002), 659–661.
[18] A. H. Nayfeh, *Order reduction of retarded nonlinear systems–the method of multiple scales versus center-manifold reduction*, Nonlinear Dyn., *51* (2008), 483–500.
[19] A. H. Nayfeh, *The method of normal forms*, John Wiley & Sons, 2011.
[20] P. C. Rech, *Self-excited and hidden attractors in a multistable jerk system*, Chaos Solitons Fractals, *164* (2022), 112614.
[21] A. Sambas, S. Vaidyanathan, S. Zhang, M. A. Mohamed, Y. Zeng, and A. T. Azar, *A new 3-d chaotic jerk system with a saddle-focus rest point at the origin, its active backstepping control, and circuit realization*, in Backstepping Control of Nonlinear Dynamical Systems, Elsevier, 2021, pp. 95–114.
[22] P. P. Singh and B. K. Roy, *Pliers shaped coexisting bifurcation behaviors in a simple jerk chaotic system in comparison with 21 reported systems*, IFAC-PapersOnLine, *55*(1) (2022), 920–926.
[23] C. H. Skiadas and Y. Dimotikalis, *13th Chaotic Modeling and Simulation International Conference*, Springer, 2022.
[24] Y. Song and J. Wei, *Bifurcation analysis for chen's system with delayed feedback and its application to control of chaos*, Chaos Solitons Fractals, *22*(1) (2004), 75–91.
[25] S. Vaidyanathan, *Analysis, control, and synchronization of a 3-D novel jerk chaotic system with two quadratic nonlinearities*, Kyungpook Math. J., *55*(3) (2015), 563–586.
[26] S. Vaidyanathan, *A seven-term novel 3-D jerk chaotic system with two quadratic nonlinearities and its adaptive backstepping control*, in Advances in Chaos Theory and Intelligent Control, Springer, 2016, 581–607.
[27] S. Vaidyanathan, A. T. Azar, I. A. Hameed, K. Benkouider, E. Tlelo-Cuautle, B. Ovilla-Martinez, C.-H. Lien, and A. Sambas, *Bifurcation analysis, synchronization and FPGA implementation of a new 3-d jerk system with a stable equilibrium*, Mathematics, *11*(12) (2023), 2623.
[28] S. Vaidyanathan, K. Benkouider, and A. Sambas, *A new multistable jerk chaotic system, its bifurcation analysis, backstepping control-based synchronization design and circuit simulation*, Arch. Control Sci, *32*(1) (2022), 123.
[29] S. Vaidyanathan, E. Tlelo-Cuautle, K. Benkouider, A. Sambas, and B. Ovilla-Martínez, *FPGA-based implementation of a new 3-d multistable chaotic jerk system with two unstable balance points*, Technologies, *11*(4) (2023), 92.
[30] Z. Wei, *Delayed feedback on the 3-D chaotic system only with two stable node-foci*, Comput. Math. Appl., *63*(3) (2012), 728–738.
[31] E. Zambrano-Serrano and A. Anzo-Hernández, *A novel antimonotic hyperjerk system: Analysis, synchronization and circuit design*, Phys. D: Nonlinear Phenom., *424* (2021), 132927.
[32] R. Zhang, *Bifurcation analysis for T system with delayed feedback and its application to control of chaos*, Nonlinear Dyn., *72*(3) (2013), 629–641.